Journal of Oceanography, Vol. 62, pp. 667 to 680, 2006

Impacts of Frontal Stability and Topography on Cross-Shelf Exchange in the Northern Gulf of Mexico

NADYA T. VINOGRADOVA[1]* and DMITRI A. NECHAEV[2]

[1]*Atmospheric and Environmental Research (AER), Inc., Lexington, MA 02421, U.S.A.*
[2]*The University of Southern Mississippi, Stennis Space Center, MS 39529, U.S.A.*

(Received 20 July 2005; in revised form 18 May 2006; accepted 23 May 2006)

The shelfbreak wintertime thermal front in the Northeastern Gulf of Mexico often exhibits meandering, eddy formation and warm-water intrusion. A high level of frontal variability plays an essential role in exchange processes across the shelf. This study examines the impacts of local frontal instability and bottom topography on turbulent heat exchange across the front using the results of two numerical models. Analysis of a series of numerical experiments reveals that the flow is baroclinically unstable. Predicted frontal instability contributes significantly to cross-frontal exchange and accounts for about 35% of the total eddy heat flux. Onshore eddy heat flux has the highest intensity at the frontal position. In addition, eddy activity and heat flux are sensitive to variation of bottom topography. For topographic features and frontal characteristics that are typical of the area, bottom steepness enhances the flux and is nearly proportional to the cross-frontal heat exchange. The study attempts to explain physical mechanisms that drive frontal circulation in the area and to quantify heat transport across the shelf. Estimated heat fluxes can provide important information for climate and ecosystem modeling of the Mississippi Bight.

Keywords:
· Shelfbreak front,
· turbulent heat exchange,
· baroclinic instability,
· Gulf of Mexico.

1. Introduction

There is a commonly observed front located near the continental shelf break in the Northeastern Gulf of Mexico offshore of the Louisiana, Mississippi, Alabama and Florida coasts (Cochrane and Kelly, 1986). The front separates shelf water from slope water and establishes a sharp change in water properties such as temperature, salinity, nutrients, and chlorophyll concentration. The shelfbreak front is a highly dynamic feature that often meanders. The meanders can grow to large amplitude and eventually pinch off to form rings and eddies. A typical example of the wintertime surface front observed in the Mississippi Bight is shown in Fig. 1. As shown in the AVHRR satellite image, the wintertime front separates relatively cool shelf water from relatively warm slope water, following isobathic contours. As seen from Fig. 1, there is a high level of mesoscale and sub-mesoscale variability, including a warm water intrusion, meanders, and eddies. Oceanographic analysis of a two-year database of in-situ measurements also indicates extremely variable conditions in the Mississippi Bight region (Vinogradov *et al.*, 2004). High frontal variability has significant impacts on the distribution of physical properties, including heat, momentum, oxygen, sound speed, sediments, nutrients, carbon and possible pollutants both along and across the shelf (Walsh *et al.*, 1988; Gawarkiewicz and Chapman, 1991).

The goal of this study is to characterize frontal flow and to quantify cross-frontal exchange of heat in the Northeastern Gulf of Mexico. In particular, the primary objective is to examine the impacts of local frontal instability and bottom topography on eddy heat transport in the area. There is substantial evidence suggesting that one of the major causes of frontal variability and cross-frontal water exchange is frontal instability (Joyce, 1980; Barth, 1994; Gawarkiewicz and Chapman, 1995; Lozier *et al.*, 2002). One source of instability is the potential and kinetic energy that is stored in fronts (Boss and Thompson, 1999). Growing instabilities lead to the development of meanders and the formation of cyclonic and anticyclonic eddies, which become a source of turbulent (eddy) transport (Csanady and Hamilton, 1988). Eddy transport is usually accompanied by the exchange of potential energy and momentum between eddies and mean flow (Orlanski and Cox, 1973; Ikeda, 1981). The transport of tracers, especially heat transport induced by the eddy field, has received considerable attention recently

* Corresponding author. E-mail: nadya@aer.com

Copyright©The Oceanographic Society of Japan/TERRAPUB/Springer

because of its role in total heat budget and climate processes (Gent and McWilliams, 1990; Stammer, 1998; Wunsch, 1999). Understanding how eddies could transport water properties is essential due to their significant impact on boundary currents and coastal circulation (Jayne and Marotzke, 2002).

Along with local frontal instability, the presence of changing bottom topography is another factor that influences the dynamics of frontal flow (Orlanski, 1969; Hsueh and Cushman-Roisin, 1983; Chapman and Gawarkiewicz, 1995, 1997; Gawarkiewicz and Chapman, 1995; Jiang and Garwood, 1995, 1996; Kikuchi and Wakatsuchi, 1999). Depending on what kind of topography is considered, it can have both stabilizing and destabilizing effects. Quasi-geostrophic modeling by Chao (1990), Reszka and Swaters (1999), Mechoso and Sinton (1981) and laboratory experiments by Wolfe (2003) suggest that a steep bottom slope is essential for instability of fronts with an interface that is inversely correlated with topographic slope. Three-dimensional cases with outcropping fronts studied by Jiang and Garwood (1995, 1996), and Chapman and Gawarkiewicz (1995) show that a steady flow of dense shelf water becomes dynamically unstable when it is being transported over the slope. Gawarkiewicz and Chapman (1995) conclude that steep slopes lead to more rapid offshore transport of dense shelf water by eddies.

Previous studies show that evolution of the front is extremely sensitive to a number of factors, such as the position of the front, the shape and the depth of the frontal interface, bottom steepness and width of the shelf. Different combinations of these factors can alter frontal stability in opposing ways. Therefore, the contribution of topography should be considered with regard to the unique frontal characteristics and typical topographic features of the area. Mississippi Bight bathymetry is characterized by a relatively gentle continental slope region at the west and a steep shelfbreak at the east, including the DeSoto canyon region (Fig. 2). As seen in Fig. 1, alongshore variation of the bathymetry modifies the position and the dynamics of the frontal flow. The eastern side of the shelfbreak front is more variable than the western end. However, the western side of the domain is often characterized by an intrusion of warm water (Fig. 1), which might account for additional cross-shelf water exchange.

2. Methods

Frontal dynamics and cross-frontal exchange are examined through a series of idealized numerical experiments using the Estuarine and Coastal Ocean Model (ECOM). Frontal instability is simulated in a cyclic channel using a characteristic front as a reference state. The choices of frontal characteristics, stratification, and topography represent typical wintertime conditions in the Mississippi Bight and are based on observations collected in support of the Northeastern Gulf of Mexico Physical

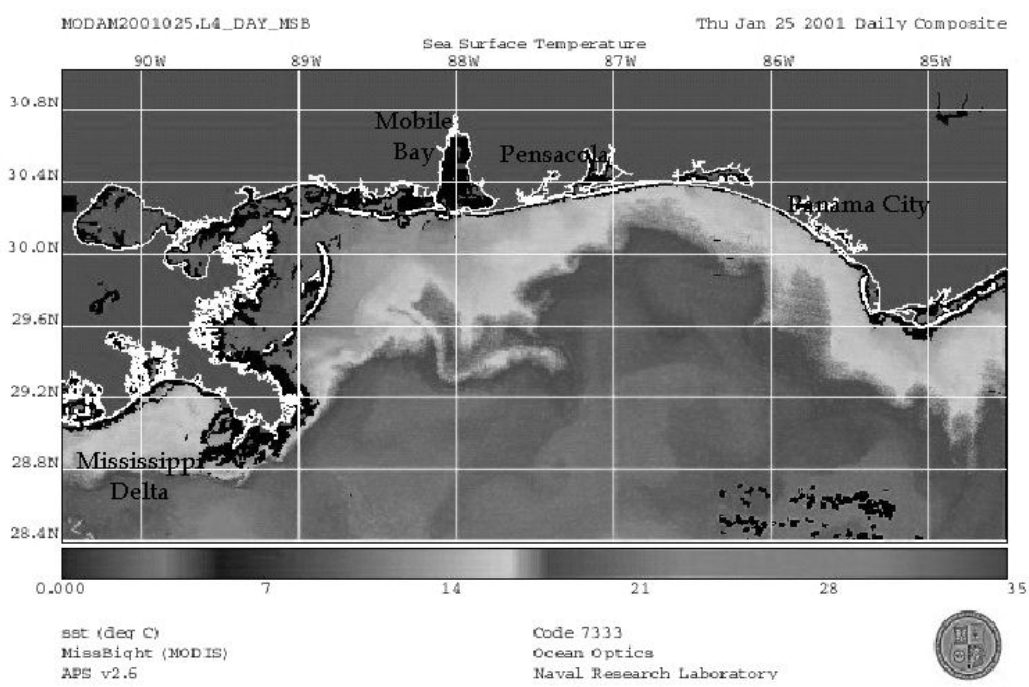

Fig. 1. NRL AVHRR satellite image of winter temperature front in the Mississippi Bight at January 25, 2001.

Oceanography Program (NEGOM). The vertical structure of the front is shown in Fig. 3. Cold shelf waters are separated from warmer, slightly stratified slope water by a transition region at the shelfbreak. The shelfbreak front extends from the surface down to a depth of 50 m. Although the shelf water is both colder and fresher than the slope water, temperature variations dominate in the density distribution, making the slope water the less dense of the two water masses.

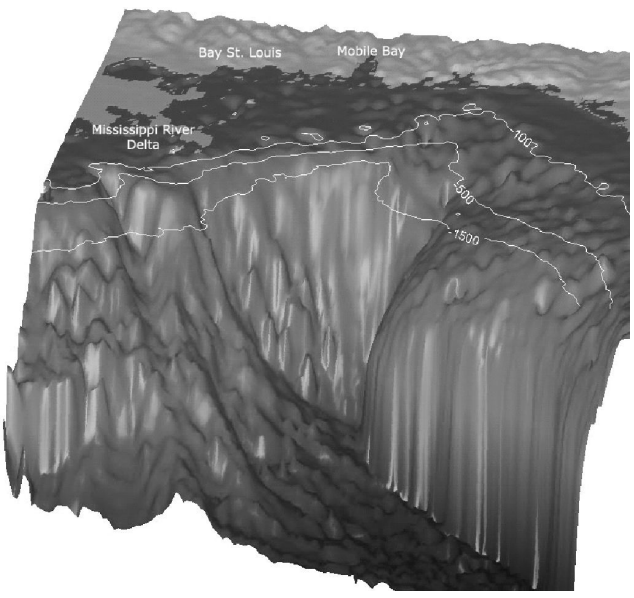

Fig. 2. Mississippi Bight bathymetry.

The ECOM is initialized with the observed cross-frontal temperature and salinity distributions (Fig. 3) and geostrophically adjusted velocities. The model is integrated for a 30-day period to allow meanders to develop. The 30-day integration is a sufficient period for the analysis of frontal instabilities and eddy development (Griffiths *et al.*, 2000). Instability is examined in terms of meander growth and eddy formation. To establish whether the meanders predicted by the model are baroclinic, the energetics are analyzed. Following the approach described in Orlanski and Cox (1973), the energy is partitioned into three components: potential energy, mean kinetic energy and eddy kinetic energy. Interchanges among these three forms of energy are calculated at every time step during model integration.

Assuming the product of seawater density, ρ_0, and specific heat, C_p, is relatively constant, velocity-temperature covariance reflects the eddy heat flux. Consequently, the turbulent heat fluxes across the front are calculated as the space and time average of the product of the perturbation velocity and the perturbation temperature

$$C_p \rho_0 \overline{v'T'} \tag{1}$$

where v' and T' are deviations from the temporal- and spatial-mean cross-frontal velocity and temperature. To compute temperature-velocity covariance (1), the same averaging is used as in computations of v' and T'. The values of the mean density and specific heat are chosen as ρ_0 = 1024 kg/m^3 and C_p = 4000 J/kg°C. The cross-frontal heat flux is computed according to Eq. (1) at every

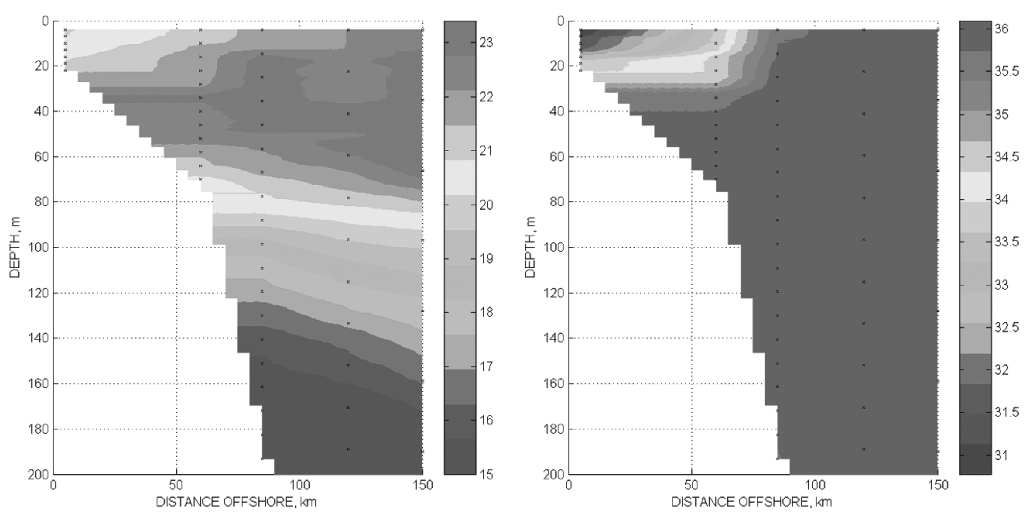

Fig. 3. Vertical structure of wintertime shelfbreak front in the Mississippi Bight. Cross-section of temperature (left) and salinity (right) are based on the NEGOM data.

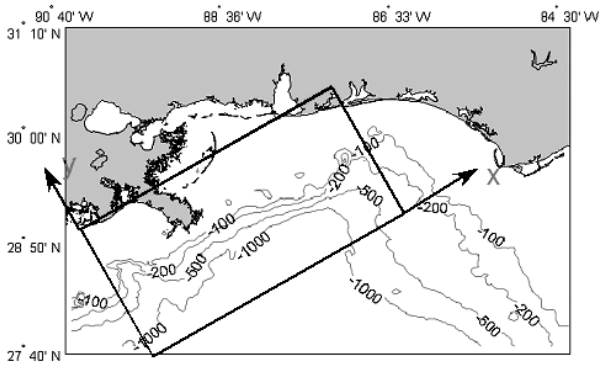

Fig. 4. Mississippi Bight area and the ECOM model domain for the idealized numerical experiments.

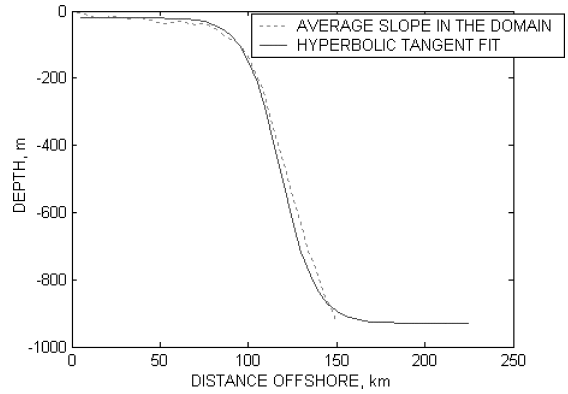

Fig. 5. Hyperbolic tangent fit to the Mississippi Bight average bathymetry.

time step to analyze temporal variability of the heat exchange. To estimate the average heat flux across the front, a monthly averaged heat flux is calculated based on the computed time series.

To investigate the effect of the topography on the frontal dynamics and cross-frontal exchange, five different representations of the ECOM bathymetry are considered with varying bottom slope steepness. The magnitudes of the slopes are chosen to be representative of the western (gentle) and eastern (steeper) sides of the Mississippi Bight bathymetry. For each topographic experiment, analysis of energetics and cross-frontal exchange are performed according to the procedure mentioned above. Finally, the results predicted by the idealized model are compared with the results of more realistic model experiments in order to identify similar physical mechanisms that control frontal dynamics. Realistic calculations are based on the results of the real-time Intra-Americas Sea Ocean Nowcast/Forecast System or IASNFS, designed at the Naval Research Laboratory at the Stennis Space Center, MS (Martin, 2000; Ko *et al.*, 2003).

3. Experiment Design

Frontal stability and cross-frontal heat exchange is studied through a series of simplified numerical experiments using the ECOM. The ECOM is a three-dimensional, time dependent, sigma coordinate, free surface model, designed by HydroQual, Inc. Previous studies prove the ECOM to be a useful tool for studying oceanography in the Mississippi Bight (Vinogradova *et al.*, 2005), as well as for simulating dynamics of other continental regions such as the Oregon continental shelf (Allen *et al.*, 1995), Massachusetts Bay (Blumberg *et al.*, 1993), and Georges Bank (Chen *et al.*, 1995). A detailed description of the ECOM can be found in Vinogradova *et al.* (2005) and HydroQual (2002).

In the current study the ECOM is set up to represent an ocean domain of 1-km maximum depth, 200-km width and 300-km length (Fig. 4). The *y*-coordinate represents a cross-frontal direction, the *x*-coordinate is an along-frontal direction and is aligned with isobaths in order to simplify model bathymetry. The Mississippi Bight two-minute bathymetry is shown in Fig. 2. The reference ECOM bathymetry is determined from the fit of a hyperbolic tangent function (Lozier *et al.*, 2002) to the alongshore average slope. The fit is given by:

$$h(y) = H_S + 0.5\left(H_d - H_s\right)\left(1 - \tanh\left[\frac{y - y_m}{\alpha}\right]\right) \qquad (2)$$

where H_S = 20 m is a shelf depth, H_d = 930 m is maximum domain depth, y_m = 118 km is the location of maximum slope, and α = 20 km is a lateral extent of a slope, which controls the steepness of the bottom topography. The fit is shown in Fig. 5. The ECOM bottom topography is uniform along the shelf, deepening gradually from the shallow continental shelf to the steep slope.

The ECOM horizontal resolution is 5 km. The chosen horizontal grid spacing is sufficient to resolve the Rossby radius of deformation at the Mississippi Bight shelfbreak, which is about 20–30 km (He and Weisberg, 2002). There are sixteen layers in the vertical. The vertical increment varies in thickness to accommodate more resolution near the surface and the bottom. The Coriolis parameter, *f*, is allowed to vary with *y*. As demonstrated in Wood (1988), the beta effect is important in controlling a mean flow induced by frontal disturbances.

The ECOM is initialized with a front, computed based on the NEGOM wintertime observations and shown in Fig. 3. Twenty levels in the vertical are chosen to represent the initial state of the front. No external forcing is applied to the reference configuration of the model. It is worth noting that in previous studies (e.g., Gawarkiewicz and Chapman, 1995), numerical simulations were per-

formed with a highly idealized front, while in this study an observed front is imposed on the model. The background (constant) vertical mixing is 1×10^{-6} m^2/s. The constant value used in Smagorinsky's formula for horizontal mixing is 1×10^{-1} (non-dimensional). The ratio of viscosity to diffusivity (Prandtl number) is 1.0 for both horizontal and vertical mixing. The internal time step is 60 seconds and the external step is 6 seconds, which gives numerically stable solutions for the type of calculation reported here.

The boundary conditions in the vertical are the conditions at the free surface and the bottom of the basin. The zero surface flux boundary condition is applied to the ECOM domain. On the bottom there is no flow normal to the bottom of the basin and the fluxes of heat and salt are zero. The bottom frictional stresses are determined from the logarithmic law of the wall (HydroQual, 2002). The bottom friction coefficient is set to 2.5×10^{-2}; the bottom roughness is 3×10^{-3} m. Rigid wall boundaries at the northern and southern boundaries and cyclic boundary conditions at the east and west sides are applied.

Sensitivity to the bottom topography is analyzed through a sequence of five experiments with varying bottom topography steepness. For each representation, the maximum depth of the channel stays the same (H_d = 930 m), whereas the magnitude of the slope increases progressively. The slopes are referred to as gentle, medium, reference, large, and steep. The steepness of the slope is regulated by varying parameter α in Eq. (2). Decreasing the parameter α makes the slope steeper. The range of the parameter α and corresponding value of the bottom slope are shown in Table 1. The magnitudes of the slopes are chosen to be representative of the western (gentle) and eastern (steeper) sides of the Mississippi Bight bathymetry. After the circulation is geostrophically adjusted to the initial density distribution, the ECOM is run for a 30-day period for all topographic experiments.

Table 1. Parameter α for a hyperbolic tangent function on the bottom topographies in Eq. (2) and corresponding values of the bottom slopes.

Experiment	Bottom slope	α
Gentle slope (GS)	8.9×10^{-3}	40
Medium slope (MS)	11.9×10^{-3}	30
Reference (basic) slope (BS)	17.9×10^{-3}	20
Large slope (LS)	23.9×10^{-3}	15
Steep slope (SS)	35.9×10^{-3}	10

4. Effect of Local Frontal Instability

4.1 Geostrophic adjustment

Each ECOM experiment begins from rest. In order for the system to attain the velocity field that is consistent with the specified temperature and salinity distributions, the ECOM is run diagnostically for 15 days. Figure 6A shows the adjustment phase during the reference experiment. During this period the initial zero surface elevation gradually adjusts toward the prescribed density distribution. Cold and dense shelf waters have lower surface elevation compared to warmer and lighter slope water. A distance 100 km offshore corresponds to the location of the model shelfbreak. Figure 6A demonstrates that the maximum gradient of the surface elevation occurs at the location of the shelfbreak, which is consistent with the location of the prescribed temperature front.

As can be seen from Fig. 6B, a 15-day period is sufficient for the adjustment. Initial zero velocities become geostrophic. A steady geostrophic current is formed after day 10 of diagnostic integration. The current is aligned with the front and flows eastward. The geostrophic velocities of about 25 cm/s are similar to those observed by Golubev and Hsueh (2002) in the Mississippi Bight area.

4.2 Frontal instabilities and energetics

The ECOM is initialized with the front shown in Fig. 7A, revealing geostrophic velocities and elevation, and integrated for a 30-day period. After 10–15 days of integration the initially zonal structure of the surface front is perturbed and a wavelike disturbance develops (Fig. 7B). Notice too that the width of the front narrows. Once established, the meanders continue to grow toward the end of the integration (Fig. 7C). By the end of integration, the dominant feature is a strong anticyclonic circulation with associated warm eddies on the deep side of the front. The initially geostrophic along-shelf current becomes a narrow meandering jet flowing eastward. Figure 7 also illustrates the vertical evolution of the front. During the integration, deep slope water is upwelled onto the shelf (Figs. 7B and C). Topographic upwelling is also supported by computed upward vertical velocities.

To understand the nature of the disturbances it is useful to look at the energetics of the system. This analysis is similar to that described by Orlanski and Cox (1973). The fields are decomposed into an along-channel average (x-coordinate) and deviation from this field, henceforth referred to as mean and eddy fields, respectively. A mean quantity is denoted by an overbar and a deviation (eddy) component is denoted by a prime. The same averaging procedure is applied to the ECOM equations of motion, which results in a new system of equations for eddy quantities. Integrating new equations over the total volume yields the evolution equation for the total kinetic energy of the perturbation flow:

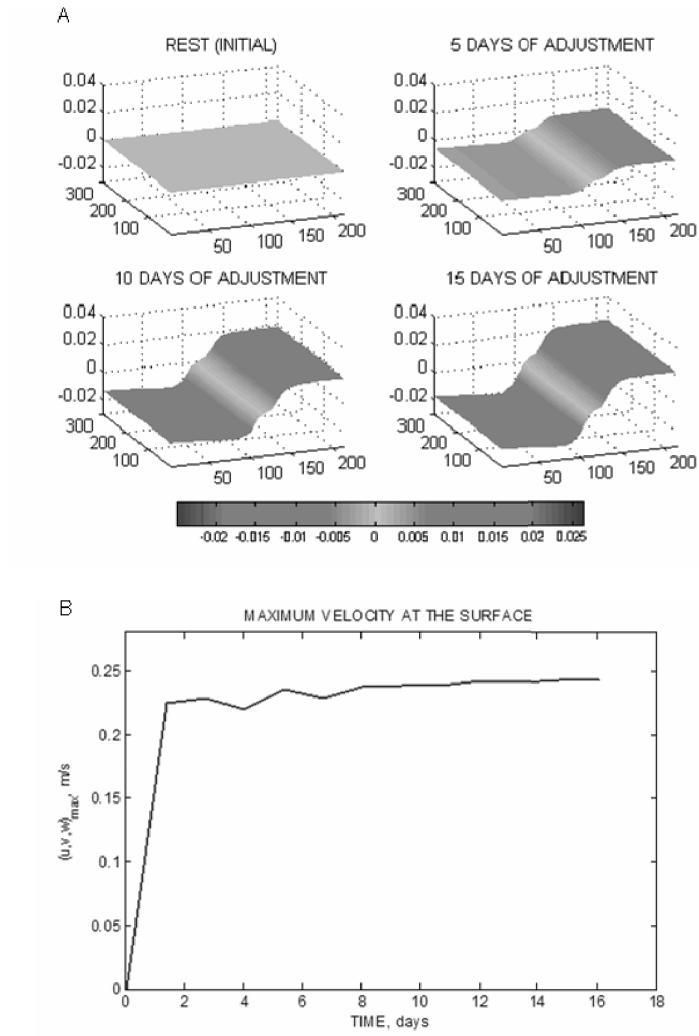

Fig. 6. Reference run: (A) surface elevation and (B) surface circulation during the geostrophic adjustment phase.

$$\frac{d}{dt}\iiint \frac{u'^2+v'^2}{2}dV$$
$$= \iint\left[\bar{u}_x\overline{u'u'}+\bar{v}_x\overline{u'v'}+\bar{u}_z\overline{u'w'}+v_z\overline{v'w'}\right]dydz$$
$$-\iint g\overline{\rho'w'}dydz$$
$$-\iint\left[A_h\left[(\nabla u')^2+(\nabla v')^2\right]+A_v\left[(u_z')^2+(v_z')^2\right]\right]dydz \quad (3)$$

where (u', v', w') is deviation of the velocity field from the along-channel average, subscripts denote partial derivatives, ρ' is density perturbation and A_v, A_h are coefficients of vertical and horizontal diffusion, respectively. For mathematical details of the energy terms derived for the ECOM equations see Vinogradova (2004).

The interpretation of (3) is that the time rate of change of eddy kinetic energy is the sum of: (i) conversion of mean to eddy kinetic energy by Reynolds stresses; (ii) conversion of potential to eddy kinetic energy; and (iii) loss of energy by dissipation. In Eq. (3) the energy is partitioned into three components: potential energy (*PE*), mean kinetic energy (*MKE*), and eddy kinetic energy (*KE′*). Total kinetic energy is expressed as the sum of the mean and eddy kinetic energy. Potential energy is expressed as a total gravitational potential energy in the usual way (for example, see Wood (1988) or Orlanski and Cox (1973)):

$$TKE = \iiint \rho_0\left(\frac{\bar{u}^2+\bar{v}^2}{2}\right)dV + \iiint \rho_0\left(\frac{u'^2+v'^2}{2}\right)dV$$
$$= MKE + KE' \quad (4)$$

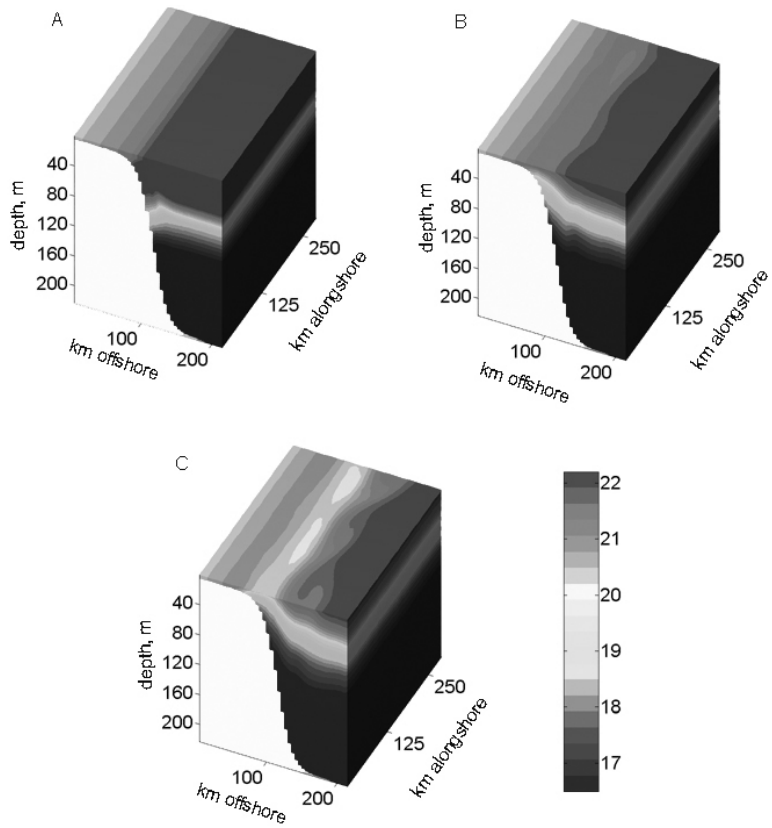

Fig. 7. Reference run: Temperature in the upper 200 m of the ECOM model. (A) initial conditions based on the CTD observations; (B) 15 and (C) 30 days after initialization.

$$PE = \iiint \frac{g}{\rho_0} \rho z dV. \tag{5}$$

To analyze the nature of disturbances, each energy component and interchanges among these three forms are computed at every time step according to Eqs. (3)–(5). Figure 8 (middle panel) shows a 30-day time series of total potential and kinetic energy computed according to (4) and (5). Potential energy drops during integration due to lack of supply to the system and due to diffusion of heat and salt. Total kinetic energy continues to grow toward the end of integration. Note that magnitude of potential energy is considerably larger (of the order of 10^4) than kinetic energy. Total energy of the system follows the descending trend of the potential energy, which implies that a certain amount of energy is lost through dissipation. The evolution of mean and eddy kinetic energy is shown in the upper panel of Fig. 8. Kinetic energy of the mean flow decreases with time, while kinetic energy of the perturbation flow increases steadily as meanders grow.

The bottom panel of Fig. 8 shows interchanges between system energetics computed according to Eq. (3). Analysis of energetics shows hybrid baroclinic-barotropic instability of the flow. During the first week of the ECOM integration, fluctuations are clearly baroclinic: they extract potential energy from the system by transferring it from the mean to eddy potential energy, and then convert it to eddy kinetic energy. The baroclinic conversion term is large. As potential energy decreases, the baroclinic term declines. After 10–15 days meanders are established and the barotropic conversion term comes into play. A negative barotropic term represents a transfer of energy from eddy to mean flow by Reynolds stresses. However, due to the decline of mean kinetic energy and small values of the barotropic conversion term, intensification of mean flow by eddies is not significant. The energetics and life cycle presented here are similar to those found by Griffiths *et al.* (2000), Wood (1988), and Ikeda (1981).

4.3 Cross-frontal exchange

Cross-frontal exchange is computed according to Eq. (1) at 50 m depth, which is the depth of the seasonal thermocline determined from observations (Fig. 3). Heat flux for the reference experiment is shown in Fig. 9. A position of zero on the *x*-axis corresponds to the position

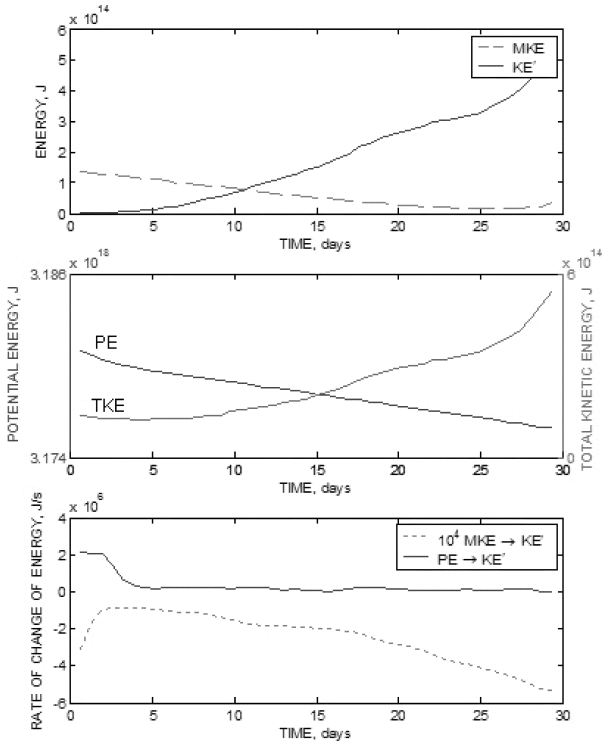

Fig. 8. Reference experiment: time series of the energy components and the energy conversion terms.

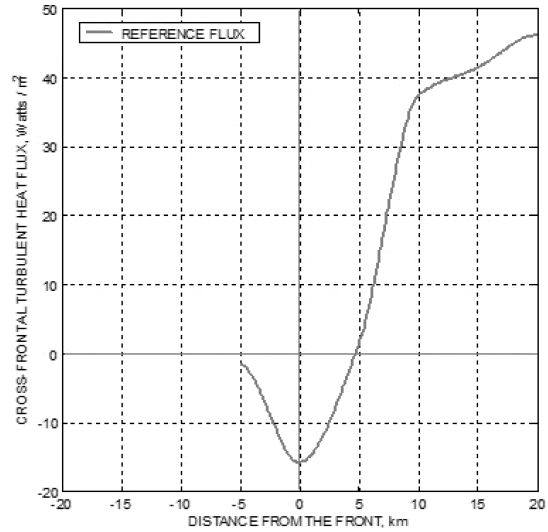

Fig. 9. Reference experiment: Monthly mean turbulent heat flux at the thermocline depth (50 m).

of the front, which is determined as a point of maximum temperature gradient across the shelf. The values of the flux are negative to the left of the front and positive to the right, indicating a cross-frontal exchange between the shelf and slope waters. Furthermore, temperature perturbations are negative, $T' < 0$, on the cold shelf. Thus, negative values of heat flux imply transport of cold water offshore, since the positive direction of velocity is chosen offshore. In addition, maximum exchange occurs at the position of the front (Fig. 9), indicating that the shelfbreak front enhances turbulent heat transport across the shelf.

5. Topographic Effects

5.1 Meander development

In the reference experiment described above the ECOM topography represents an average bathymetry in the Mississippi Bight. Sensitivity of frontal stability and heat flux to different bathymetric features is examined in the following section. In particular, the impacts of bottom steepness on frontal dynamics are the subject of interest. Figure 10 shows the temporal evolution of the surface front during 30 days of integration with four types of bottom topography:

(1) Sea surface elevation over the gentle slope has the greatest magnitude at the start of integration (Fig. 10, gentle slope, day 1). However, as opposed to the reference experiment, the amplitude of the cross-frontal difference in the surface elevation decreases as integration continues. Toward the end of integration a weak anticyclonic eddy starts to develop with a diameter of about 10 km (Fig. 10, gentle slope, day 30).

(2) Similar to the case of gentle topography, during the first days of integration sea surface elevation over the medium slope decreases slightly on the deep side of the surface front (Fig. 10, medium slope day 1–15). However, in contrast to the case with the gentle topography, surface elevation rises as integration continues. By the end of integration, rising surface elevation forms a long wave with an amplitude of about 20 cm. An eddy starts to develop on the top of this wave (Fig. 10, medium slope, day 30). The eddy amplitude of 25 cm is smaller than the 40 cm during reference experiment.

(3) Surface circulation over the large slope is different from the previous two cases. The cross-shelf gradient of surface elevation increases during the whole period of integration (Fig. 10, large slope, day 1–30) in a similar manner as it does during reference experience. The surface front meanders and several anticyclonic eddies are formed. The eddy diameters are about 20–25 km, which are bigger than the 10–20 km eddies found in the experiments with the gentle and medium slopes. By the end of integration the amplitudes of anticyclonic eddies grow up to 60 cm (Fig. 10, large slope, day 30), which is larger than 40 cm found during the reference run. In addition, several cyclonic eddies are formed on the shallow side of the front (Fig. 10, large slope, day 30) with amplitudes of 40 cm.

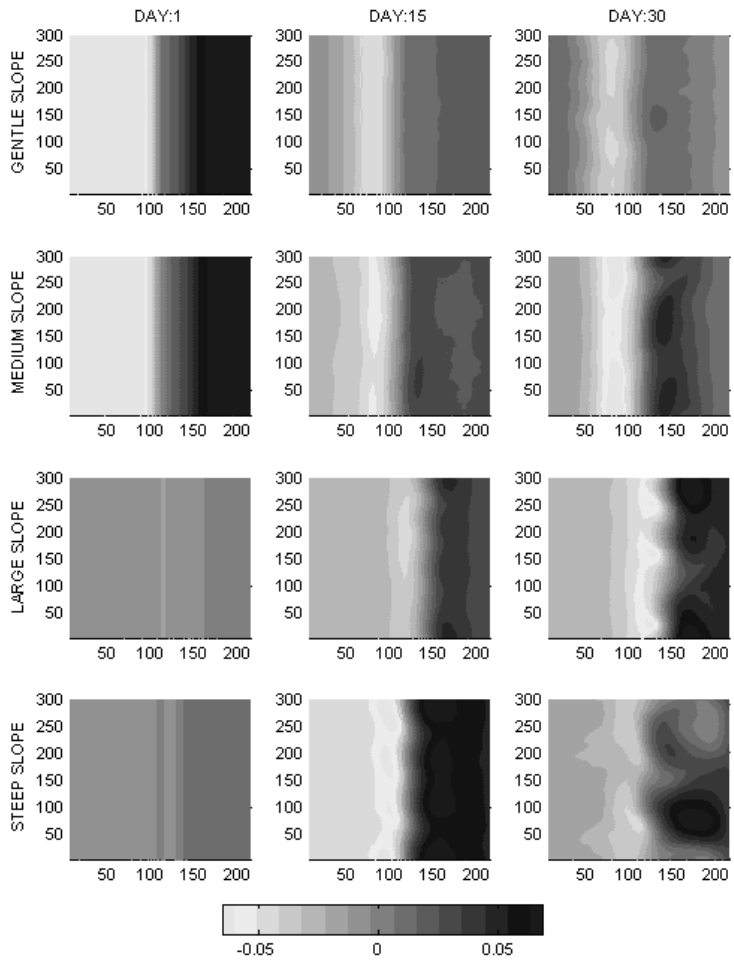

Fig. 10. Topographic experiment: sea-surface elevation over various bottom topographies during 30 days of integration.

(4) Surface elevation over the steepest topography has the smallest amplitude at the start of integration (Fig. 10, steep slope, day 1). As integration continues, the cross-shelf gradient of elevation increases rapidly and reaches the maximum amplitude of 60 cm on both sides of the front (Fig. 10, steep slope, day 15). Instabilities at the surface develop as rapidly as the growth of the surface elevation amplitude. By day 30 the initial strong zonal flow is greatly disturbed (Fig. 10, steep slope, day 30). Both cyclonic and anticyclonic surface meanders are built up. In addition, by this time meanders begin to travel, which did not happen in the other topographic experiments.

5.2 Cross-frontal exchange

Figure 11A and Table 2 show absolute values of mean flux at the frontal position relative to the bottom steepness. Figure 11B examines the relative change of mean front flux with respect to steepness. The *x*-axis is the ratio of the different slopes relative to the reference slope. The smallest ratio (0.5) is the ratio of the gentle to reference slope. The largest ratio (2.0) is the ratio of the steep slope to the reference slope (Table 2). The *y*-axis represents the ratio of the mean fluxes for the different slopes relative to the reference flux.

Mean values of the flux gradually increase as the slope gets steeper (Fig. 11A). Note the linear relation between the increase of the slope and the increase of the mean frontal flux for the experiments with the gentle, medium and reference slopes (dashed line in Fig. 11B). The slope of this line is equal to one. When the bottom slope is reduced by 50% from the reference to the gentle slope, i.e. changing from a slope value of 17.9×10^{-3} to 8.9×10^{-3}, the value of the mean frontal heat flux is also reduced by 50%, dropping from a value of 15.8 W/m^2 to of 7.7 W/m^2. A similar relation is observed for the ex-

periment with the medium slope. The bottom slope is reduced by 30% from the reference (17.9×10^{-3}) to the medium slope (11.9×10^{-3}). This leads to a 30% decrease of the frontal flux. The 15.8 W/m^2 value for the reference flux decreases to 10.3 W/m^2 during the medium slope experiment.

The situation is different when the bottom slope is increased relative to the reference slope (Fig. 11B). There is no linearity between the ratios of fluxes for the reference, large and steep slope events. The increase of the bottom slope of 30%, from the reference slope 17.9×10^{-3} to the large slope 23.9×10^{-3}, leads to a 130% increase of the frontal flux from a value of 15.8 W/m^2 to 35.9 W/m^2. Another increase of the bottom steepness, from the reference slope 17.9×10^{-3} to the steep slope 35.9×10^{-3}, i.e. an increase of 100%, results in a 210% increase of the frontal flux, reaching the maximum value of 49.0 W/m^2. In spite of a positive correlation between the bottom steepness and flux values, the relation in nonlinear. The steeper the slope, the more flux diverges from the dashed line in Fig. 11B.

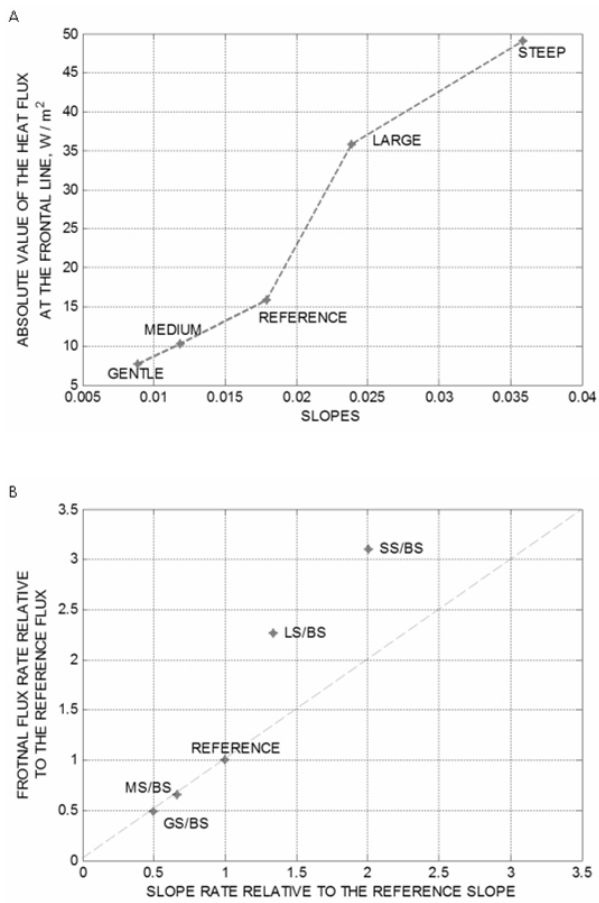

Fig. 11. (A) Absolute values of the cross-frontal heat flux at the thermocline depth (50 m) at the position of the front and (B) rate of change of the frontal fluxes and seafloor slopes.

6. Comparison with Realistic Model

The effects of local frontal instability and bottom topography on cross-frontal exchange predicted by an idealized model are compared with the results of the NRL realistic experiments. Figure 12 shows monthly mean surface temperature based on the results of the realistic experiments (NRL model). The temperature front is located near the shelfbreak at a depth of 50–70 m with a mean temperature value of 18.2°C (white line). To compare the cross-frontal fluxes of the ECOM idealistic and NRL realistic models, the NRL model flux is computed along a characteristic transect shown by dark dots in Fig. 12. The line of this slice goes across the shelf. The positive direction of this slice, $\vec{n}$, coincides with the direction of the temperature gradient, i.e. offshore. Similar to the definition of the ECOM heat flux defined by formula (1), cross-frontal turbulent heat flux of the NRL model is then calculated as:

$$C_p \rho_0 \overline{V_n' T'} \tag{6}$$

where T' is the perturbation temperature along this slice and V_n' is the perturbation velocity in the direction of this slice. Values of the mean density and specific heat are chosen similar to those used in the computation of the ECOM heat flux. The top of the seasonal thermocline along the characteristic slise of the NRL model is at a

Table 2. Absolute value of the mean cross-frontal heat fluxes at the thermocline depth, computed at the position of the front; and ratio of the bottom slopes and the mean frontal fluxes relative to the reference state.

Experiment	Frontal flux value, W/m^2	Bottom slope ratio	Frontal flux ratio
Gentle slope (GS)	7.7	0.5	0.5
Medium slope (MS)	10.3	0.7	0.7
Reference (basic) slope (BS)	15.8	1	1
Large slope (LS)	35.9	1.3	2.3
Steep slope (SS)	49.0	2.0	3.1

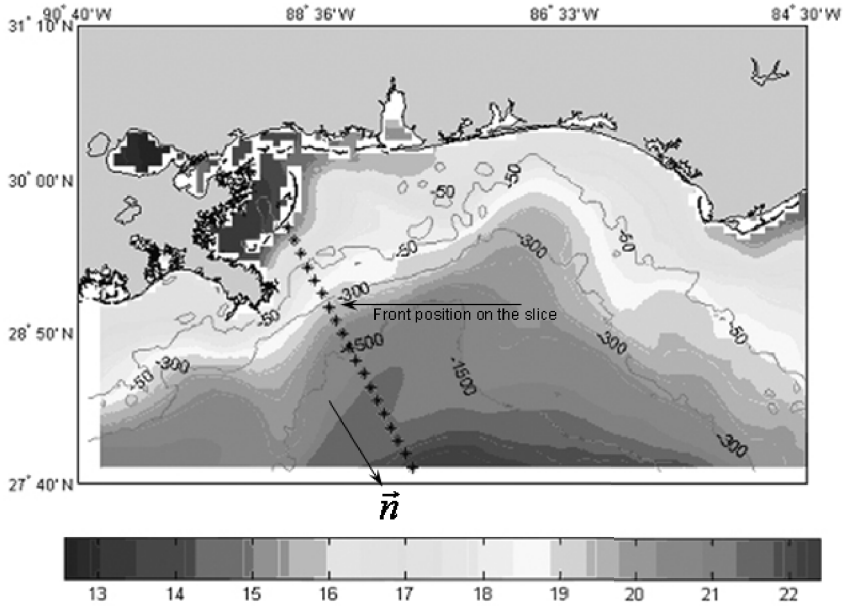

Fig. 12. Monthly mean surface temperature based on the results of the NRL model (January 2003, data courtesy Drs. Ko and Preller, NRL). $\vec{n}$ is the vector of the cross-frontal direction (direction of the slice). Positive direction of $\vec{n}$ coincides with the positive direction of the temperature gradient.

depth of 50–70 m, which is consistent with the thermocline in the ECOM simulations.

Figure 13 shows the cross-frontal turbulent heat flux of the NRL model computed according to Eq. (6). A position of zero on the *x*-axis represents the position of the front where it intersects the slice (see Fig. 12). Similar to the flux in the ECOM computations, shelf waters are to the left of the frontal point, whereas slope waters are to the right of the zero position. The value of the flux at the frontal point is nonzero, implying that there is heat transport across the front. Therefore, similar to the reference flux of the ECOM experiments, the front does not act as a barrier to the heat exchange between the shelf and slope.

Comparison of Fig. 9 and Fig. 13 reveals a similar behavior of idealized and realistic heat fluxes. Both graphs show offshore transport of cold water with maximum transport at the position of the front. The amplitude differences between the two fluxes range from 35% at the frontal position (15.8 W/m^2 and 45.1 W/m^2), to 37% 20-km offshore (46 W/m^2 and 122.7 W/m^2). The amplitude difference between the two estimates of heat transport may indicate the relative contribution of local instability to the realistic heat exchange. In the NRL realistic simulation heat flux is influenced by many factors including, for example, variability of the wind, while in the idealized experiments heat flux is induced by local frontal instability only. To examine this possibility, the mean characteristics of both models solutions are compared. Analysis of mean quantities is necessary in order to ensure that the disturbances in both systems are of the same kind. The background (mean) currents, which undergo instabilities, should be similar in both models.

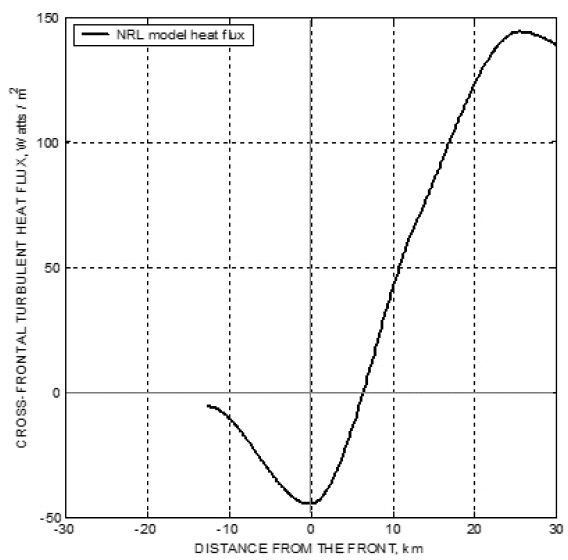

Fig. 13. Monthly mean cross-frontal turbulent heat flux for the NRL model transect, computed at the depth of thermocline. Position of the front (zero on *x*-axis) is shown in Fig. 12.

Monthly mean velocities simulated by the NRL

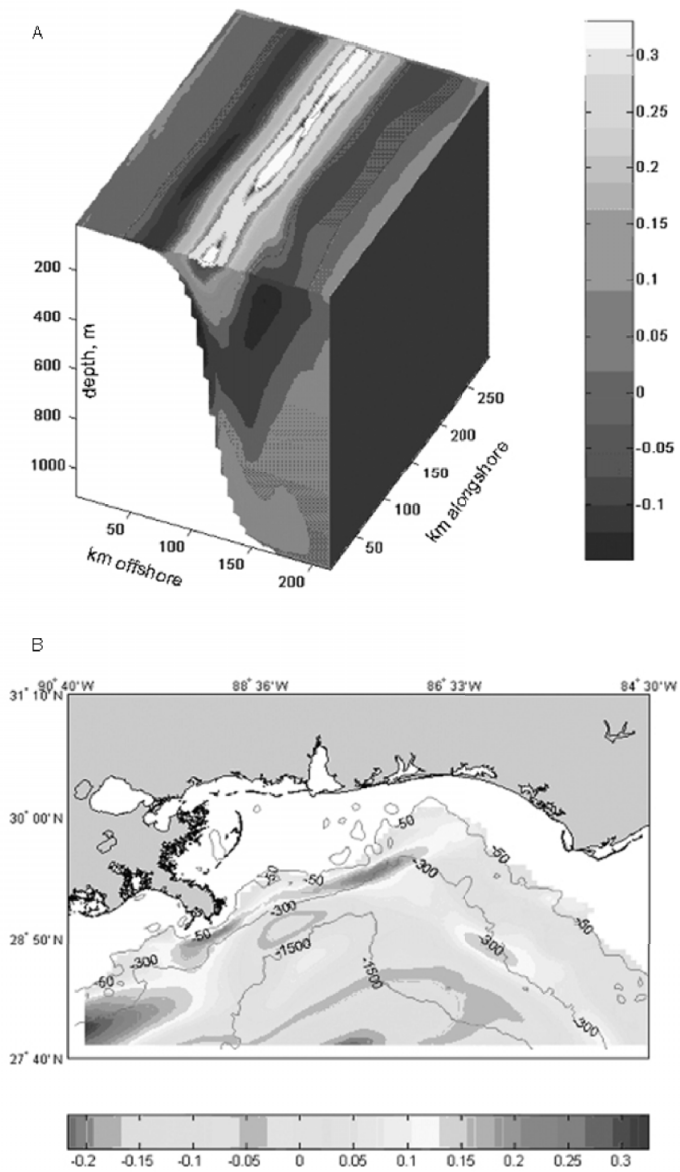

Fig. 14. (A) Reference experiment: Monthly mean along-front velocity for the ECOM experiment. (B) Monthly mean u-component of the horizontal velocity of the NRL model at the thermocline depth, 50 m.

model and the ECOM are estimated. The resemblance between the mean currents in idealized and realistic model is demonstrated in. Figure 14A shows a monthly mean *u*-component of the horizontal velocity for the ECOM experiment. The background flow in the ECOM is an eastward flow, aligned with the front (positive *x*-direction). The speed of the current is about 0.3 m/s at the surface. It is located near the shelfbreak and extends up to 300 m vertically. Surface and thermocline values of the background current in the NRL model are shown in Fig. 14B. Aligned with the front shown in Fig. 12, this current also flows eastward with a speed of 0.3 m/s at the surface. Since the background flows are similar in both models, the assumption about disturbances of the ECOM and NRL model is valid. Therefore, comparison of Fig. 9 and Fig. 13 provides information about the contribution of frontal instability to cross-frontal exchange, which is about 35% of the total eddy heat flux.

The bottom slope/heat flux relation predicted by the ECOM idealized experiments is also compared with the NRL realistic model results. The cross-frontal turbulent heat flux is computed along two cross sections shown in Fig. 15A. One transect is located over the gentle slope (left line) and another transect intersects the front on the

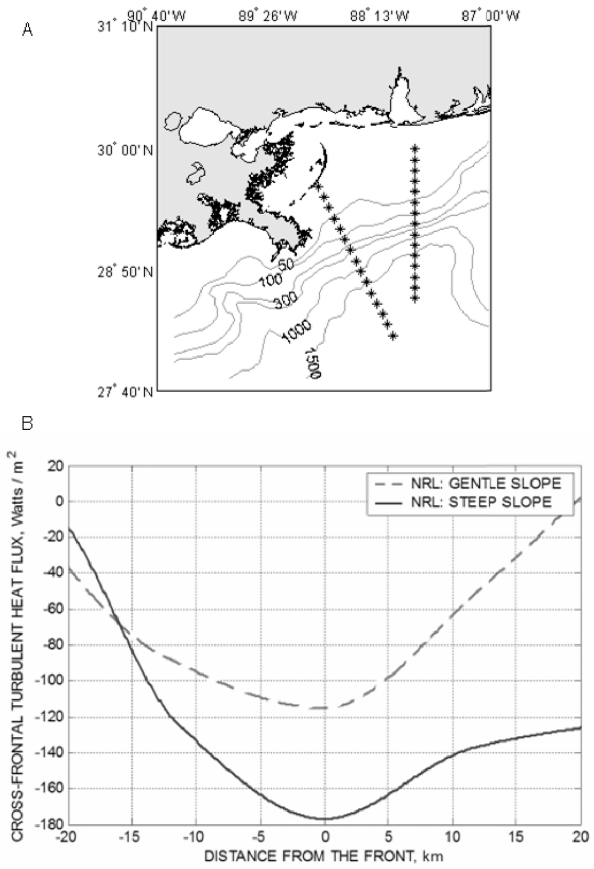

Fig. 15. (A) Position of the topographic slices extracted from the NRL model and (B) cross-frontal turbulent heat fluxes along the two slices.

steep side of the domain (right line). Heat fluxes are computed in a similar manner as described in Section 5. They correspond to the same model time and are shown in the bottom panel of Fig. 15. Zero on the *x*-axis is the position where the transect line intersects the temperature front. The behavior of the heat flux observed in the ECOM experiments is consistent with that revealed by the NRL model. The value of the flux at the frontal position across the steep slope is greater (~180 W/m^2) than that across the gentle slope (~100 W/m^2). The positive correlation between the magnitude of the NRL heat flux and bottom steepness agrees with the ECOM results.

7. Summary and Discussion

The results show that in the Mississippi Bight the shelfbreak front is unstable, so even small perturbations grow into eddies that transport water across the shelf. The initial flow undergoes three phases of development. The adjustment process during the first stage is followed by meander development and growth during the second phase. Eddy detachment or even jet annihilation in the simulations is the third phase of the flow development. In the real ocean, atmospheric conditions such as cooling during winter, maintain the front, whereas in the simulations the front is eventually destroyed due to the lack of external forcing.

Analysis of energetics suggests that baroclinic instabilities are dominant. During the baroclinic phase, eddy kinetic energy increases at the expense of potential energy, which is initially stored in the density field. When meanders are developed, the barotropic phase begins, which is associated with eddy-mean flow interactions within the frontal zone. The computed barotropic term shows that the net energy transfer is from eddies to mean flow by Reynolds stresses, which suggests that fluctuations could be important to the intensification of the mean current. Eddy-to-mean energy flux in the Northern Gulf of Mexico was also documented by Webster (1965), who analyzed surface velocity data in the Florida Current.

Comparison between realistic and idealized simulations shows that the contribution of local frontal instability (baroclinic and barotropic) to total heat flux is about 35%–37%. In both models, the values of the flux reach their extreme (negative) amplitudes at the position of the front, implying that the front does not act as a barrier but rather enhances the exchange of heat across the shelf.

The presence of sloping topography affects both frontal stability and heat exchange across the front. There is a positive correlation between the increase of bottom steepness and flux values. The steepness-flux relation is linear if bottom topography is gentler than average. The fluxes exhibit a nonlinear increasing trend with steeper bottom slope. Over steep topography eddies develop fast and move offshore rapidly, enhancing the exchange of heat across the shelf. For the cold shelf water a sloping bottom provides an additional gravitational acceleration component, which modifies eddy dynamics (Gawarkiewicz and Chapman, 1995). The effect is stronger as the topography becomes steeper. Steeper bottom slopes lead to more rapid offshore movement of eddies, therefore enhancing cross-frontal water exchange. This was clearly seen in the experiment with the steepest slope, when eddies reach their finite amplitudes and pinch off. Topographic effects predicted by the idealized model are supported by the realistic simulations.

Acknowledgements

The authors are grateful to Dong-Shang Ko and Ruth Preller (NRL/SSC) for making their model output available. Two anonymous reviewers helped to clarify major points of the manuscript. This work was supported by the ONR grant N00014-00-1-0201 and NSF grant OCE-01-18200.

References

Allen, J. S., P. A. Newberger and J. Federiuk (1995): Upwelling circulation on the Oregon continental shelf. *J. Phys. Oceanogr.*, **25**, 1843–1866.

Barth, J. A. (1994): Short-wavelength instabilities on coastal jet and fronts. *J. Geophys. Res.*, **99**, 16095–16115.

Blumberg, A., R. Signell and H. Jenter (1993): Modeling transport processes in the coastal ocean. *J. Environ. Eng.*, **1**, 31–52.

Boss, E. and L. Thomson (1999): Mean flow evolution of a baroclinically unstable potential vorticity front. *J. Phys. Oceanogr.*, **29**, 273–287.

Chao, S.-Y. (1990): Instabilitites of fronts over a continental margin. *J. Geophys. Res.*, **95**, 3199–3211.

Chapman, D. C. and G. Gawarkiewicz (1995): Offshore transport of dense shelf water in the presence of a submarine canyon. *J. Geophys. Res.*, **100**, 13,373–13,387.

Chapman, D. C. and G. Gawarkiewicz (1997): Shallow convection and buoyancy equilibrium in an idealized coastal polynya. *J. Phys. Oceanogr.*, **27**, 555–566.

Chen, C., R. C. Beardsley and R. Limeburner (1995): A numerical study of stratified tidal rectification over finite-amplitude banks, Part II: Georges Bank. *J. Phys. Oceanogr.*, **25**, 2111–2128.

Cochrane, J. D. and F. J. Kelly (1986): Low-frequency circulation on the Texas–Louisiana continental shelf. *J. Geophys. Res.*, **91**, 10645–10659.

Csanady, G. T. and P. Hamilton (1988): Circulation of slopewater. *Cont. Shelf Res.*, **8**, 565–624.

Gawarkiewicz, G. and D. C. Chapman (1991): Formation and maintenance of shelfbreak fronts in an unstratified flow. *J. Phys. Oceanogr.*, **21**, 1225–1239.

Gawarkiewicz, G. and D. C. Chapman (1995): A numerical study of dense water formation and transport on a shallow, sloping continental shelf. *J. Geophys. Res.*, **100**, 4489–4507.

Gent, P. R. and J. C. McWilliams (1990): Isopycnal mixing in ocean circulation model. *J. Phys. Oceanogr.*, **20**, 150–155.

Golubev, Y. and Y. Hsueh (2002): Low-frequency variability of surface currents on the Northeastern Gulf of Mexico (NEGOM) shelf. Final Report, US Department of Interior, MMS, New Drleans, LA, p. 78–93.

Griffiths, C., M. Ikeda and P. C. Smith (2000): A numerical model comparison of baroclinic instability in the presence of topography. *Tellus. Series A: Dynamic Meteorology and Oceanography*, **52A**, 42–65.

He, R. and R. H. Weisberg (2002): A Loop Current intrusion case study on the West Florida shelf. *J. Phys. Oceanogr.*, **33**, 465–477.

Hsueh, Y. and B. Cushman-Roisin (1983): On the formation of surface to bottom fronts over steep topography. *J. Geophys. Res.*, **88**, 743–750.

HydroQual (2002): A Primer for ECOMSED. Version 1.3, 188 pp.

Ikeda, M. (1981): Meanders and detached eddies of a strong eastward flowing jet using a two layer quasigeostrophic model. *J. Phys. Oceanogr.*, **11**, 526–540.

Jayne, S. R. and J. Marotzke (2002): The oceanic eddy heat transport. *J. Phys. Oceanogr.*, **32**, 3328–3345.

Jiang, L. and R. W. Garwood, Jr. (1995): A numerical study of three-dimensional dense bottom plumes on a Southern Ocean continental slope. *J. Geophys. Res.*, **100**, 18,471–18,488.

Jiang, L. and R. W. Garwood, Jr. (1996): Three-dimensional simulation of outflows on continental shelf. *J. Phys. Oceanogr.*, **26**, 1214–1233.

Joyce, T. M. (1980): On production and dissipation of thermal variance in the ocean. *J. Phys. Oceanogr.*, **10**, 460–463.

Kikuchi, T. and N. Wakatsuchi (1999): A numerical investigation of the transport process of dense shelf water from a continental shelf to a slope. *J. Geophys. Res.*, **104**, 1197–1210.

Ko, D. S., R. H. Preller and P. J. Martin (2003): An experimental real-time Intra-Americas Sea Ocean Nowcast/Forecast System for coastal prediction. Fifth Conference on Coastal Atmospheric and Oceanic Prediction and Processes, August 6–8, 2003, Seattle, Washington.

Lozier, M. S., M. S. C. Reed and G. G. Gawarkiewicz (2002): Instability of a shelfbreak front. *J. Phys. Oceanogr.*, **32**, 924–944.

Martin, P. J. (2000): Description of the Navy Coastal Ocean Model Version 1.0. Tech. Rep. NRL/FR/7322-00-9962, 42 pp.

Mechoso, C. R. and D. M. Sinton (1981): Instability of baroclinic flows with horizontal shear along topography. *J. Phys. Oceanogr.*, **11**, 813–821.

Orlanski, I. (1969): The influence of bottom topography on the stability of jets in a baroclinic fluid. *J. Atmos. Sci.*, **26**, 1216–1232.

Orlanski, I. and M. D. Cox (1973): Baroclinic instability in ocean currents. *Geophys. Fluid Dyn.*, **3**, 297–332.

Reszka, M. K. and G. E. Swaters (1999): Eddy formation and interaction in a baroclinic frontal geotrophic model. *J. Phys. Oceanogr.*, **29**, 3025–3042.

Stammer, D. (1998): On eddy characteristics, eddy transports, and mean flow properties. *J. Phys. Oceanogr.*, **28**, 727–739.

Vinogradov, S., N. Vinogradova, V. Kamenkovich and D. Nechaev (2004): Temperature and salinity variability in the Mississippi Bight. *MTS Journal*, **38**(1), 52–60.

Vinogradova, N. T. (2004): Instability of shelf-break fronts and cross-shelf exchange in the Northern Gulf of Mexico. Ph.D. dissertation, University of Southern Mississippi, U.S.A., 252 pp.

Vinogradova, N., S. Vinogradov, D. Nechaev, V. Kamenkovich, A. F. Blumberg, Q. Ahsan and H. Li (2005): Evaluation of the Northern Gulf of Mexico Littoral Initiative (NGLI) model based on the observed temperature and salinity in the Mississippi Bight Shelf. *MTS Journal*, **39**(2), 25–38.

Walsh, J. J., P. E. Biscaye and G. T. Csanady (1988): The 1983–1984 Shelf Edge Exchange Processes (SEEP)-I Experiment: Hypothesis and highlight. *Cont. Shelf Res.*, **8**, 435–456.

Webster, F. (1965): Measurement of eddy fluxes of momentum in the surface layer of the Gulf Stream. *Tellus*, **17**, 239–245.

Wolfe, C. L. (2003): Eddy generation by flow over variable topography. *WHOI Geophysical Fluid Dynamics Summer School Proceedings*, **2003**, 172–190.

Wood, R. A. (1988): Unstable waves on oceanic fronts: Large amplitude behavior and mean flow generation. *J. Phys. Oceanogr.*, **18**, 775–787.

Wunsch, C. (1999): Where do ocean eddy heat fluxes matter. *J. Geophys. Res.*, **104**, 13,235–13,249.